

International Journal of Modern Physics D
 © World Scientific Publishing Company

CONSTRAINTS ON THE HIGH-DENSITY NUCLEAR EQUATION OF STATE FROM NEUTRON STAR OBSERVABLES

DAVID BLASCHKE

*Instytut Fizyki Teoretycznej, Uniwersytet Wrocławski, pl. M. Borna 9, 50-204 Wrocław, Poland
 Bogoliubov Laboratory for Theoretical Physics, JINR, 141980 Dubna, Russia
 blaschke@ift.uni.wroc.pl*

THOMAS KLÄHN

*Physics Division, Argonne National Laboratory, Argonne, Illinois 60439-4843, USA
 thomas.klaehn@googlemail.com*

FRIDOLIN WEBER

*Dept. Physics, San Diego State University, 5500 Campanile Drive, San Diego, CA 92182, USA
 fweber@sciences.sdsu.edu*

Received Day Month Year
 Revised Day Month Year
 Communicated by Managing Editor

Depending on the density reached in the cores of neutron stars, such objects may contain stable phases of novel matter found nowhere else in the Universe. This article gives a brief overview of these phases of matter and discusses astrophysical constraints on the high-density equation of state associated with ultra-dense nuclear matter.

Keywords: Nuclear matter; Quark Matter; Equation of state; Neutron stars; Pulsars

1. Introduction

A forefront area of modern research concerns the exploration of the properties of ultra-dense nuclear matter and the determination of the equation of state (EoS)—the relation between pressure, temperature and density—of such matter. Experimentally, relativistic heavy-ion collision experiments enable physicists to cast a brief glance at hot and ultra-dense matter for times as short as about 10^{-22} seconds. This is different for neutron stars, which are observed with radio and X-ray telescopes as radio pulsars and X-ray pulsars. The matter in the cores of such objects is compressed permanently to densities that may be more ten times higher than the densities inside atomic nuclei, which make neutron stars natural astrophysical laboratories that allow for a wide range of (astro) physical studies and astrophysical phenomena (Fig. 1) linked to the properties of ultra-dense nuclear matter and its associated EoS.^{1,2,3,4,5,6,7,8,9} Of particular interest are neutron stars whose observed properties deviate significantly from the norm. Examples of such neutron stars are PSR

2 *D. Blaschke, T. Klähn, and F. Weber*

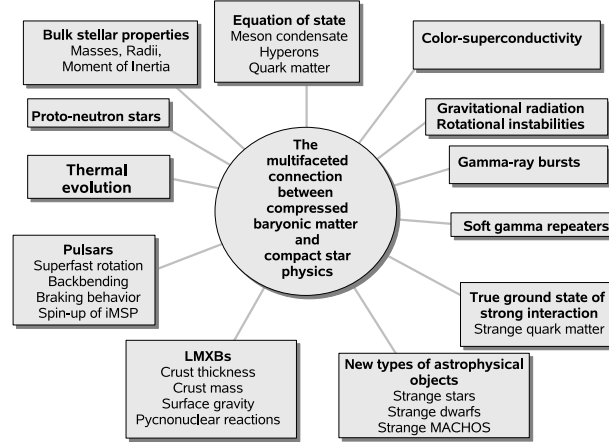


Fig. 1. The multifaceted connection between high-density nuclear matter and neutron (compact) star phenomena.⁴

J0751+1807 whose mass is $2.1 \pm 0.2 M_{\odot}$,¹⁰ neutron star RX J1856.5-3754 whose radius may be $\gtrsim 13$ km,¹¹ and XTE J1739-285 whose rotation period may be as small as 0.89 ms.¹² As discussed in this paper, such neutron star data provide an excellent opportunity to gain profound insight into the properties of nuclear matter at most extreme conditions of density.^{13,14}

2. Neutron Star Masses

Recent results of timing measurements for PSR B1516+02B, located in the globular cluster M5, imply a pulsar mass of $1.96^{+0.09}_{-0.12} M_{\odot}$ (at 68% probability) with a 95% probability that the mass of this object is above $1.68 M_{\odot}$ ¹⁵ which deviates considerably from the average masses of binary radio pulsars, $M_{BRP} = 1.35 \pm 0.04 M_{\odot}$.¹⁶ This striking result constrains neutron star masses to at least $1.6 M_{\odot}$ (2σ confidence level), and even to $1.9 M_{\odot}$ at the 1σ confidence level. The mass and structure of spherical, non-rotating neutron stars is calculated by solving the Tolman-Oppenheimer-Volkoff (TOV) equation,

$$\frac{dP(r)}{dr} = - \frac{(\varepsilon(r) + P(r))(m(r) + 4\pi r^3 P(r))}{r(r - 2m(r))}, \quad (1)$$

where $m(r) = 4\pi \int_0^r dr' r'^2 \varepsilon(r')$ is the gravitational mass inside a sphere of radius r . The baryon number enclosed by this sphere is given by

$$N(r) = 4\pi \int_0^r dr' r'^2 \left(1 - \frac{2m(r')}{r'}\right)^{-1/2} n(r'), \quad (2)$$

with $n(r)$ the baryon density profile of the star. In order to solve the TOV equation one needs to specify the stellar EoS, i.e., the relation between pressure, P ,

and energy density, ε . We apply a broad, modern collection of nuclear equations of state, which are compiled in Table 1.¹³ Each one of these models was combined at

Table 1. Collection of nuclear equations of state studied in this paper. The entries are: saturation density, n_s ; binding energy, a_V ; incompressibility, K ; skewness parameter, K' ; symmetry energy, J ; symmetry energy derivative, L ; Dirac effective mass, m_D .

EoS	n_s [fm ⁻³]	a_V [MeV]	K [MeV]	K' [MeV]	J [MeV]	L [MeV]	m_D [m]
NL ρ	0.1459	-16.062	203.3	576.5	30.8	83.1	0.603
NL $\rho\delta$	0.1459	-16.062	203.3	576.5	31.0	92.3	0.603
D ³ C	0.1510	-15.981	232.5	-716.8	31.9	59.3	0.541
DD-F4	0.1469	-16.028	220.4	1229.2	32.7	58.7	0.556
KVR	0.1600	-15.800	250.0	528.8	28.8	55.8	0.805
KVOR	0.1600	-16.000	275.0	422.8	32.9	73.6	0.800
DBHF	0.1810	-16.150	230.0	507.9	34.4	69.4	0.678
BBG	0.1901	-14.692	221.6	-132.4	36.3	79.4	—
DD-RH	0.172	-15.73	249.0	—	34.4	90.2	0.686

sub-nuclear densities with the Baym-Pethick-Sutherland EoS.¹⁷ The stellar radius, R , is defined as that stellar location where pressure vanishes, $P(R) = 0$. The star's gravitational mass and its total baryon number are thus given by $M = m(R)$ and $N = N(R)$, respectively. Most of the models shown in Table 1 are derived in the framework of the relativistic mean-field approach,^{18,19,20,21} allowing for non-linear (NL) self-interactions of the σ meson²². For model NL ρ , the isovector part of the interaction is described entirely in terms of ρ meson exchange. This is different for NL $\rho\delta$ where the isovector part of the interaction is described in terms of both ρ and δ -meson exchange. The latter is generally neglected in RMF models.²³ RMF models with density dependent input parameters (coupling constants and masses) are represented in Table 1 by four different models from two classes, where in the first one density dependent meson couplings are modeled such that several properties of finite nuclei (binding energies, charge and diffraction radii, surface thicknesses, neutron skin in ²⁰⁸Pb, spin-orbit splittings) can be fitted.²⁴ D³C additionally contains a derivative coupling which leads to momentum-dependent nucleon self-energies, and DD-F4 is modeled such that the flow constraint from heavy-ion collisions is fulfilled.²⁵ The second class of these models is motivated by the Brown-Rho scaling assumption²⁶ that not only the nucleon mass but also the meson masses should decrease with increasing density. In the KVR and KVOR models²⁷ these dependences are related to a nonlinear scaling function of the σ -meson field such that the EoS of symmetric nuclear matter and pure neutron matter below four times the saturation density coincide with those of the Urbana-Argonne group.²⁸ In this way the latter approach builds a bridge between the phenomenological RMF models and a microscopic EoS built on realistic nucleon-nucleon forces. The RMF models are contrasted with several variational models for the EoS such as APR²⁸, WFF²⁹, FPS³⁰, a relativistic Dirac-Brueckner-Hartree-Fock (DBHF) model³¹, and a non-

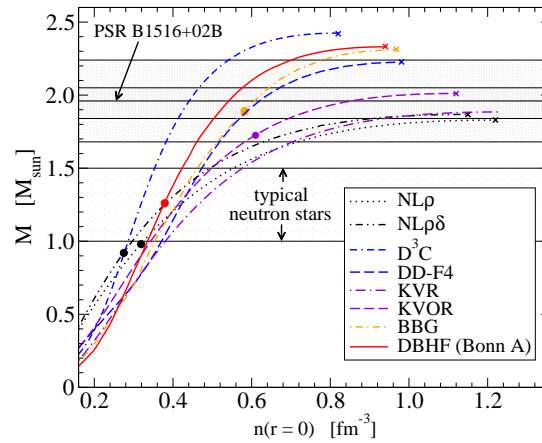


Fig. 2. Mass versus central density of neutron stars, computed from Eq. (1) for EoS shown in Table 1. Crosses refer to the maximum-mass star of each sequence, filled dots mark the critical masses and central densities beyond which the direct Urca (DU) cooling process becomes possible.

relativistic Brueckner-Bethe-Goldstone (BBG) model.³² As shown in Fig. 2, none of these values falls below the 2σ mass limit of $1.68 M_{\odot}$ for PSR B1516+02B, and even at the 1σ mass limit of $1.84 M_{\odot}$ the softest EoS $NL\rho$ and $NL\rho\delta$ cannot be excluded. We point out that if a pulsar with a mass exceeding $1.8 - 1.9 M_{\odot}$ at the 2σ or even 3σ level would be observed in the future, this would impose severe constraints on the stiffness of the nuclear EoS. For the set of EoS tested here, only the stiffest models, i.e. D^3C , DD-F4, BBG, and DBHF would remain viable candidates.

3. Gravitational Mass–Baryon Number Relation

It has been suggested that pulsar B in the double pulsar system J0737–3039 may serve to test models proposed for the EoS of superdense nuclear matter.³³ One of the interesting characteristics of this system is that the mass of pulsar B is merely $1.249 \pm 0.001 M_{\odot}$.^{34,35} Such a low mass could be an indication that pulsar B did not form in a type-II supernova, triggered by a collapsing iron core, but in a type-I supernova of an ONeMg white dwarf driven hydrostatically unstable by electron captures onto Mg and Ne.³³ The well-established critical density at which the collapse of such stars sets in is $4.5 \times 10^9 \text{ g/cm}^3$. Assuming that the loss of matter during the formation of the neutron star is negligible, a predicted baryon mass for the neutron star of $M_N = 1.366 - 1.375 M_{\odot}$ was derived in Ref. 33. This theoretically inferred baryon number range together with the star’s observed gravitational mass of $M = 1.249 \pm 0.001 M_{\odot}$ may represent a most valuable constraint on the EoS, provided the above key assumption for the formation mechanism of the pulsar B is correct.^{33,36} If so, any viable EoS proposed for neutron star matter must predict a baryon number in the range $1.366 \lesssim M_N \lesssim 1.375 M_{\odot}$ for a neutron star whose

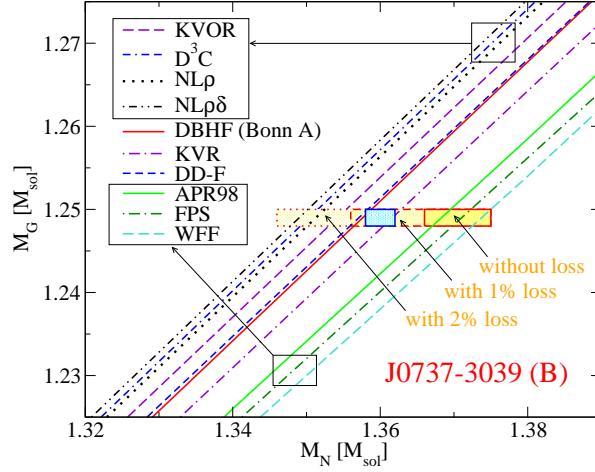


Fig. 3. Gravitational mass–baryon mass relationship³³ for PSR J0737-3039 (B) compared to a set of relativistic EoS and four nonrelativistic EoS (BBG, APR, FPS and WFF).¹³

gravitational mass is $M = 1.249 \pm 0.001 M_{\odot}$. We may contrast this result with that of an independent calculation,³⁷ where for pulsar B a baryon mass of $M_N = 1.360 \pm 0.002 M_{\odot}$ has been obtained. The authors of Ref. 33 discussed caveats such as baryon loss and variations of the critical mass due to carbon flashes during the collapse. The effect of 1% and 2% mass loss on the usefulness of this constraint to exclude model EoS is shown in Fig. 3.

4. Mass-Radius Constraints from Neutron Stars in LMXBs

Aside from neutron star masses, kilohertz quasi-periodic brightness oscillations (QPOs) seen from more than 25 neutron star X-ray binaries (LXMBs) can be used to put additional constraints on the high-density EoS. A pair of such QPOs is often seen from these systems.³⁸ In all currently viable models for these QPOs, the higher QPO frequency is close to the orbital frequency at some special radius. For such a QPO to last the required many cycles (up to ~ 100 in some sources), the orbit must be outside the star. According to general relativity theory the orbit must also be outside the innermost stable circular orbit (ISCO). Gas or particles inside the ISCO would spiral rapidly into the star, preventing the production of sharp QPOs. This implies^{39,40} that the observation of a source whose maximum QPO frequency is ν_{\max} limits the stellar mass and radius to

$$M < 2.2 M_{\odot} \frac{1000 \text{ Hz}}{\nu_{\max}} (1 + 0.75j), \quad R < 19.5 \text{ km} \frac{1000 \text{ Hz}}{\nu_{\max}} (1 + 0.2j). \quad (3)$$

The quantity $j \equiv cJ/GM^2$ (with J the stellar angular momentum) is the dimensionless spin parameter, which is typically in the range between 0.10 and 0.2 for

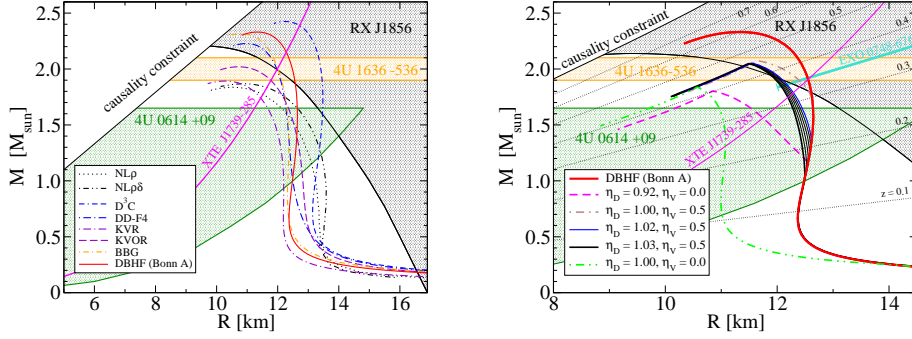


Fig. 4. Left panel: Mass-radius constraints from thermal radiation of the isolated neutron star RX J1856 (grey hatched region) and from QPOs in the LMXBs 4U 0614+09 (wedge-like green-hatched area) and 4U 1636-536 (orange hatched region). For 4U 1636-536 a mass of $2.0 \pm 0.1 M_{\odot}$ is obtained so that the weak QPO constraint would exclude the $NL\rho$ and $NL\rho\delta$ EoS, whereas the strong one renders only the stiffest EoS D^3C , $DD-F4$, BBG and $DBHF$ viable. XTE J1739-285 would favor a soft EoS, which is controversial, however (see text). Right panel: Same as left panel, but for hybrid stars with a $DBHF$ hadronic shell and a 2SC color superconducting NJL quark matter core computed for different coupling strengths, η_D and η_V . The dotted lines display surface redshifts, z , ranging from 0.1, ..., 0.7.

these systems. Equation (3) implies that for given observed value ν_{\max} the mass and radius of that source must be inside a wedge-shaped area, as shown in Fig. 4. Since wedge becomes smaller for higher ν_{\max} , the highest frequency ever observed, 1330 Hz for 4U 0614+09⁴¹, places the strongest constraint on the EoS. As can be seen from Fig. 4, the current QPO constraints do not rule out any of the EoS considered here. However, because higher frequencies imply smaller wedges, the future observation of a QPO with a frequency in the range of $\sim 1500 - 1600$ Hz would rule out the stiffest of our EoS.

If there is evidence for a particular source that a given frequency is close to the orbital frequency at the ISCO, then the mass is known to a good accuracy, with uncertainties arising from the spin parameter. This was first claimed for 4U 1820-30,⁴² but complexities in the source phenomenology have made this controversial. More recently, careful analysis of Rossi X-ray Timing Explorer data for 4U 1636-536 and other sources⁴³ has suggested that sharp and reproducible changes in QPO properties are related to the ISCO. If so, this implies that several neutron stars in low-mass X-ray binaries should have gravitational masses between $1.9 M_{\odot}$ and possibly $2.1 M_{\odot}$.⁴³ In Fig. 4 we show the estimated mass of $2.0 \pm 0.1 M_{\odot}$ for 4U 1636-536.

Recently, mass-radius constraints have been reported for the accreting compact stars XTE J1739-285⁴⁴ and SAX J1808.4-3658⁴⁵ (SAX J1808 for short) which are based on the identification of the burst oscillation frequency with the spin frequency of the compact star. It is almost impossible to fulfill the constraints from RX J1856 (and other high-mass candidates) and SAX J1808 (which favors a soft EoS) simul-

taneously so that the status of SAX J1808 is currently controversial. It is likely that the small radius estimate of Leahy et al.⁴⁵ is a consequence of the underestimation of higher harmonics when only timing data are analyzed and not also the energy spectra.⁴⁶ Neutron star XTE J1739-285 and its possible implications for the EoS are discussed in more detail below.

5. Mass-Radius Relation Constraint from RX J1856.5-3754

The nearby isolated neutron star RX J1856.5-3754 (RX J1856 for short) belongs to a group of seven objects which show a purely thermal spectrum in X-rays and in optical-UV. This allows the determination of R_∞/d , the ratio of the photospheric radius R_∞ to the distance d of the object, if the radiative properties of its photosphere are known. RX J1856 is the only object of this group which has a measured distance obtained by Hubble Space Telescope (HST) astrometry. After the distance of 117 pc⁴⁷ became known several groups pointed out that the blackbody radius of this star is as large as 15 to 17 km. Although both the X-ray and the optical-UV spectra are extremely well represented by blackbody functions they require different emission areas, a smaller hot spot and a larger cooler region. The overall spectrum could also be fitted by blackbody emission from a surface showing a continuous temperature distribution between a hot pole and a cool equator, as expected for a magnetized neutron star. The resulting blackbody radii are 17 km (two blackbodies) and 16.8 km (continuous temperature distribution)¹¹. In this paper we adopt the result of the continuous temperature fit, $R_\infty = 16.8$ km. More recent HST observations of RX J1856 indicated larger distances of up to 178 pc. A distance of around 140 pc for RX J1856 is considered a conservative lower limit.⁴⁸ For a distance of 140 pc the corresponding radius is 17 km.⁴⁹ Although some questions—in particular that of the distance—are not yet finally settled, the recent data support an unusually large radius for RX J1856.5-3754.

6. Surface Redshift

An additional test to the mass-radius relationship is provided by measurements of the gravitational redshift of line emissions from the surfaces of neutron stars. The gravitational redshift, z is given in terms of the star's gravitational mass and radius according to

$$z = 1/\sqrt{1 - 2M/R} - 1 . \quad (4)$$

In the right panel of Fig. 5, the dependence of z on star mass is shown for two representative EoS. The disputed measurement of $z = 0.35$ for EXO 0748-676^{50,51} allows for both an unconfined hadronic core composition as well as a deconfined quark-core composition.⁵² A measurement of $z \geq 0.5$ could not be reconciled with the hybrid star models suggested here, while the hadronic model would not be invalidated by redshift measurements up to $z = 0.6$.

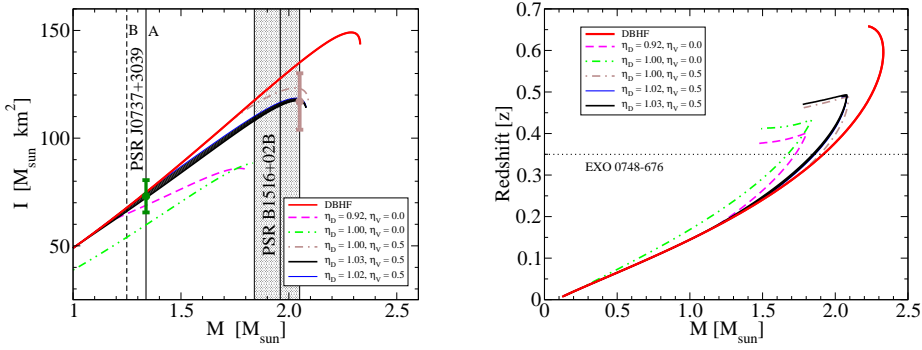


Fig. 5. Left panel: Moment of inertia versus mass. The highlighted mass regions correspond to the double pulsar J0737+3039 A+B and the pulsar B1516+02BA. Right panel: Surface redshift versus gravitational mass for a purely hadronic star (DBHF) as well as hybrid stars with 2SC color superconducting NJL quark matter cores. The dotted line labeled EXO 0748-676 displays the disputed redshift $z = 0.35$.^{50,51}

7. Moment of Inertia

The observed data of the relativistic double pulsar PSR J0737+3039 did allow a determination of the moment of inertia (MoI)^{1,2} of that star, which may be used to put further constraints on the EoS of neutron stars.^{53,54} Results for the MoI computed for the EoS of this paper are shown in Fig. 5. Due to the fact that the mass $1.338 M_\odot$ of PSR J0737+3039 A is in the vicinity of the suggested critical mass region, the quark matter core is small and the expected MoI of the hybrid star will be practically indistinguishable from that of a pure hadronic one. The situation would improve if the MoI could be measured for more massive objects, because the difference in the MoI of both alternative models for masses as high as $2 M_\odot$ could reach the 10% accuracy level.

8. Rotational Frequencies

An absolute upper limit on the spin frequency of a pulsar is given by the mass shedding limit, at which the velocity of the stellar surface equals that of an orbiting particle suspended just above the surface. For a rigid Newtonian sphere this frequency is given by the Keplerian frequency,⁵⁵

$$\nu_K = (2\pi)^{-1} \sqrt{GM/R^3} = 1833 (M/M_\odot)^{1/2} (R/10 \text{ km})^{-3/2} \text{ Hz} . \quad (5)$$

This formula was found to describe the mass shedding points for a sample of neutron star EoS extremely well.⁵⁶ However, both deformation and general relativistic effects are very important so that Eq. (5) needs to be modified. It has been found⁵⁵ that with a coefficient of 1045 Hz, Eq. (5) approximately describes the maximum rotation rate for a star of mass M and non-rotating radius R , independently of the EoS. The observation of rapidly rotating pulsars can therefore constrain the compactness and might eventually lead to the elimination of EoS that are too stiff,

since the latter lead to stars that are too big. If the recent discovery of burst oscillations with a frequency of 1122 Hz in the X-ray binary XTE J1739-285¹² and their identification with the star's spin frequency turns out to be correct, this object would spin at a rotational period of 0.89 ms, rendering it the first sub-millisecond pulsar ever observed, imposing severe constraints on the EoS. The boundary for the mass-radius relationship reads in this case⁴⁴

$$R < 9.52 (M/M_{\odot})^{1/3} \text{ km} . \quad (6)$$

As can be seen from the left panel in Fig. 4, this constraint would rule out all neutron stars of masses $M < 1.75 M_{\odot}$. Only neutron stars computed for the stiffest EoS of our collection (D³C, DD-F4, BBG and DBHF) remain viable. In concluding this section, we mention that an important test of the transport properties of the matter inside sub-millisecond pulsars arises from the r-mode instability.⁵⁷ This constraint on superconducting quark matter in neutron stars has recently been discussed for the putative sub-millisecond pulsar XTE J1739-285,⁵⁸ where it was argued that this object must be either a strange star or a quark-hadron hybrid star. In passing we mention that rotational instabilities in rotating stars, known as gravitational radiation driven instabilities, set a more stringent limit on rapid stellar rotation than mass shedding from the equator.^{1,2} These instabilities originate from counter-rotating surface vibrational modes which at sufficiently high rotational star frequencies are dragged forward. In this case gravitational radiation, which inevitably accompanies the aspherical transport of matter, does not damp the instability modes but rather drives them. Viscosity plays the important role of damping these instabilities at a sufficiently reduced rotational frequency such that the viscous damping rate and power in gravity waves are comparable. The most critical instability modes that are driven unstable by gravitational radiation are the *f*-modes and the recently discovered *r*-modes.⁶⁰ The latter may severely constrain the composition of compact stars that would rotate at sub-millisecond periods.⁵⁸

9. Mass Clustering

Compact stars in binary systems in general undergo during their evolution a stage with disc accretion leading to both, spin-up and mass increase. Initial indications for a spin frequency clustering in low-mass X-ray binary systems, reported by measurements with the Rossi-XTE, have lead to the suggestion to interpret such a correlation as a waiting-point phenomenon where star configurations cross the border between pure neutron stars and hybrid stars in the spin frequency–mass plane.⁶¹ A systematic analysis of the critical line for a deconfinement phase transition in the phase diagram for accreting compact stars⁵⁹ has revealed that the suggested population clustering due to the phase transition shall rather lead to a mass clustering effect. For strange stars, however, such an effect shall be absent.⁶² For generic polytropic forms of the EoS of quark and hadronic matter, the relationship between softness or hardness of the EoS and the structure of this phase diagram has been

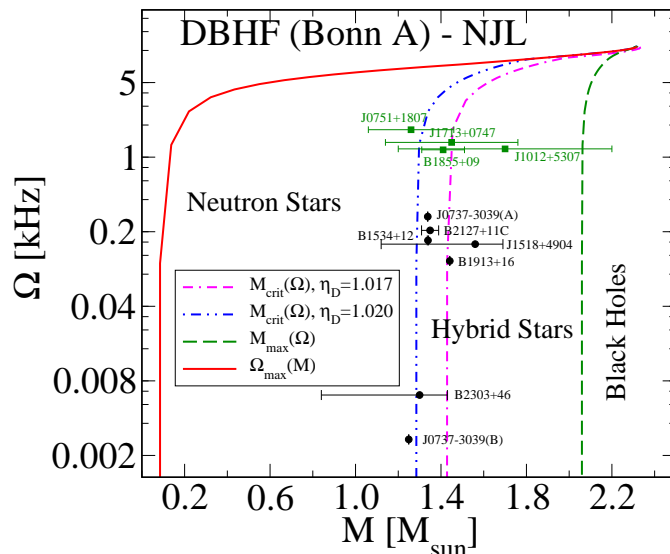


Fig. 6. Rotational frequency, Ω , versus mass, M , of neutron stars. Stable stars are located in the region bordered by the maximum rotation frequency $\Omega_{\max}(M)$, where mass-shedding from the equator occurs, and the maximum mass $M_{\max}(\Omega)$ at which gravitational instability against collapse to a black hole sets in. The dash-dotted (dash-double-dotted) line marks the onset of the generation of a quark matter core in the star's interior for a diquark coupling parameter $\eta_D = 1.020$ ($\eta_D = 1.017$), see Fig. 4 for the corresponding mass-radius relations of the non-rotating stellar sequences. The data with error bars correspond to binary radio pulsars (black dots) and neutron stars with a white dwarf binary (green squares). The correlation of the distribution of objects with the line for a deconfinement phase transition could be interpreted as a waiting point phenomenon during the accretion evolution of the compact stars (mass clustering).⁵⁹

demonstrated in Ref. 63. For the specific example of the DBHF hadronic EoS and a color superconducting stiff quark matter EoS, we show the phase diagram of rotating compact stars in Fig. 6. For curiosity we show also the masses and spin frequencies for compact stars in binary radio pulsars and neutron star–white dwarf binaries and observe an interesting correlation of the distribution of these objects with the critical deconfinement phase transition line for diquark coupling $\eta_D = 1.02$. There might be other reasons for the mass clustering of spinning pulsars,⁶⁷ but the suggestion to relate it to a phase transition in the interior can not be excluded. If true, it would be a strong constraint for the hybrid EoS and suggest a critical density for deconfinement in compact stars at about 0.4 fm^{-3} (i.e., $2.5 n_s$). We want to point out that the non-zero quark chemical potential ($\mu \neq 0$) domain is a rather poorly understood region of the QCD phase diagram. Fundamental approaches, like solving the in-medium QCD Schwinger-Dyson equations in a specific QCD model^{68,69,70} to obtain a quark matter EoS are demanding. This well justifies the description of

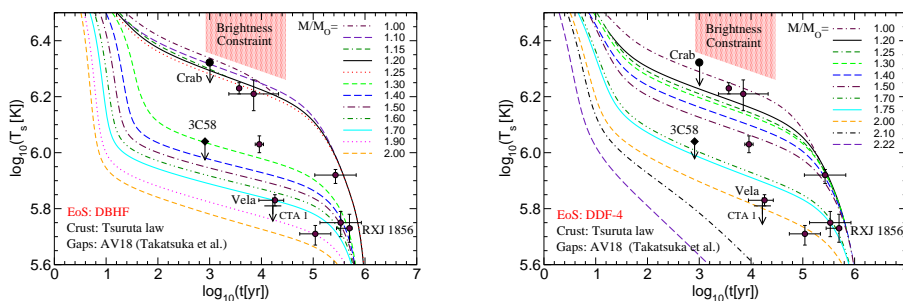


Fig. 7. Hadronic star cooling curves for DBHF (left) and DDF-4 (right) model EoS. Different lines correspond to compact star mass values indicated in the legend (in units of M_{\odot}), data points with error bars are taken from Ref. ⁶⁴. The hatched trapeze-like region represents the brightness constraint (BC).⁶⁵ The onset of the DU process entails a high sensitivity of TA curves to small mass variations known as DU problem⁶⁶.

a quark matter phase within three-flavor NJL-type models, giving access even to diquark pairing channels at reasonable expense.^{71,72,73,74}

10. Stellar Cooling

Neutron stars cool for the first 10^5 years through neutrino emission from their cores, which is followed at later times by photon emission. We simulate this behavior by using the cooling code developed in Refs. ^{75, 76}. The cooling calculations are performed for different hadronic EoS, different assumptions about superconductivity, and different stellar crust models. Moreover, we try to use consistent microscopic inputs. (For systematic field-theoretical approaches to the neutrino cooling problem in neutron stars see, for instance, Ref. ^{77, 5, 78, 79}.) The main neutrino cooling processes in hadronic matter are the direct Urca (DU), the medium modified Urca (MMU) and the pair breaking and formation (PBF). For quark matter, the main cooling processes are the quark direct Urca (QDU), quark modified Urca (QMU), quark bremsstrahlung (QB) and quark pair formation and breaking (QPFB)⁸⁰. Also the electron bremsstrahlung (EB), and the massive gluon-photon decay⁸¹ are included.

The 1S_0 neutron and proton gaps in the hadronic shell are taken according to the calculations in Ref. ⁸² corresponding to the thick lines in Fig. 5 of Ref. ⁷⁵. However, the 3P_2 gap is suppressed by a factor 10 compared to the BCS model calculation in Ref. ⁸², consistent with arguments from a renormalization group treatment of nuclear pairing.⁸³ Without such a suppression of the 3P_2 gap the hadronic cooling scenario would not fulfill the TA constraint.⁸⁴

The possibilities of pion condensation and of other so called exotic processes are included in the calculations for purely hadronic stars but do not occur in the hybrid star calculations since the critical density for pion condensation exceeds that for

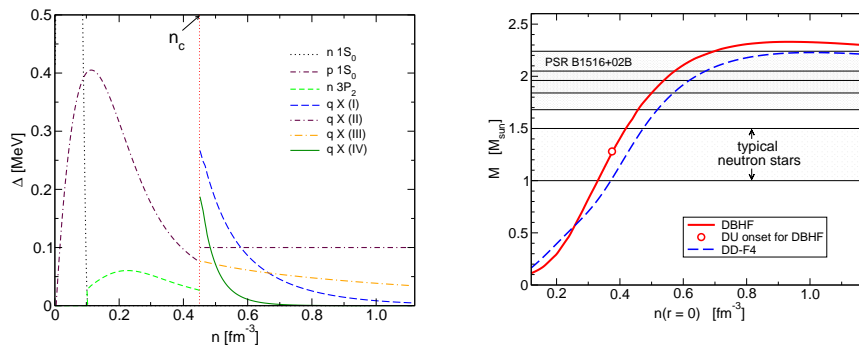
12 *D. Blaschke, T. Klähn, and F. Weber*


Fig. 8. Density dependence of the pairing gaps in nuclear matter together with that of the hypothetical X-gap in quark matter (left). Mass–central density relation for the two hadronic EoS models DBHF and DD-F4 (right). The dot indicates the onset of the DU process.

deconfinement in our case.⁷⁵ While the hadronic DU process occurs in the DBHF model EoS for all neutron stars with masses above $1.27 M_\odot$, it is not present at all in the DD-F4 model, see the right panel of Fig. 8. We account for the specific heat and the heat conductivity of all particle species whose presence is predicted by β -equilibrium. In addition, in the case of quark matter the contributions of massless and massive gluon-photon modes are taken into account too.

In the 2SC phase only the contributions of quarks forming Cooper pairs (say red and green) are suppressed via huge diquark gaps, while those of the remaining unpaired blue color lead to a so fast cooling that the hybrid cooling scenario becomes unfavorable.⁸⁵ We thus assume the existence of a weak pairing channel such that in the dispersion relation of hitherto unpaired blue quarks a small residual gap can appear. We call this gap Δ_X and show that for a successful description of the cooling scenario Δ_X has to have a density dependence. We have studied the ansatz $\Delta_X = \Delta_0 \exp[-\alpha(\mu/\mu_c - 1)]$, where μ is the quark chemical potential, $\mu_c = 330$ MeV. For the analyses of possible models we vary the values of α and Δ_0 , given in the Table 1 of Ref. 86 and shown in the left panel of Fig. 8.

11. Temperature-Age (TA) Test

We consider the cooling evolution of young neutron stars with ages $t \sim 10^3 - 10^6$ yr which is governed by the emission of neutrinos from the interior for $t \lesssim 10^5$ yr and thermal photon emission for $t \gtrsim 10^5$ yr. The internal temperature is on the order of $T \sim 1$ keV. This is much smaller than the neutrino opacity temperature $T_{\text{opac}} \sim 1$ MeV as well as the critical temperatures for superconductivity in nuclear ($T_c \sim 1$ MeV) or quark matter ($T_c \sim 1 - 100$ MeV). Therefore, the neutrinos are not trapped and the matter is in a superconducting state. In Fig. 8 we show the density dependence of the pairing gaps in nuclear matter^{82,75} together with those of the hypothetical X-gap in quark matter.^{87,85,86} The phase transition occurs at

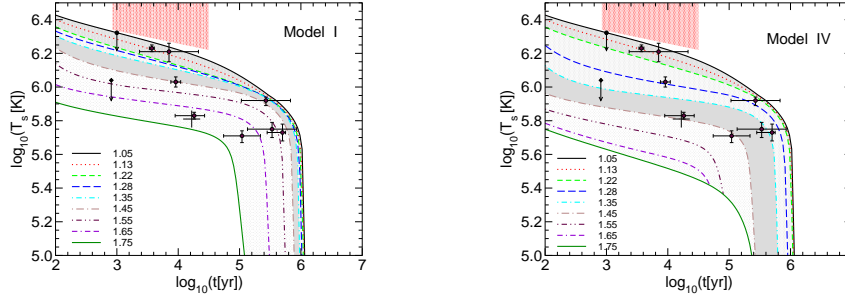


Fig. 9. Cooling curves for hybrid star configurations with 2SC+X pairing pattern and X-gap model I (left) versus model IV (right). For the gaps see the left panel of Fig. 7. The grey value for the shading of the mass bin areas corresponds to the probability for that mass bin value in the population synthesis model of Ref. 88, for details see Ref. 66.

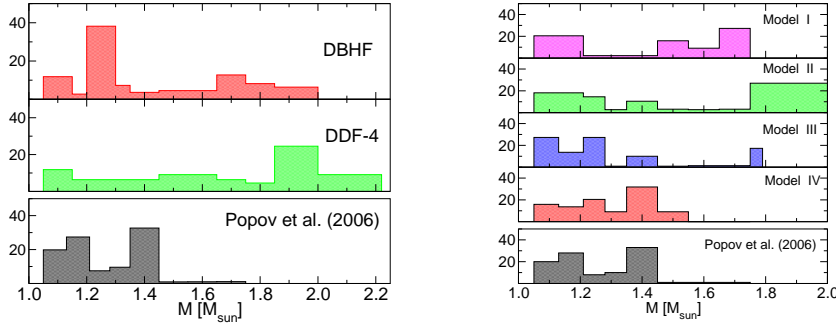


Fig. 10. NS mass spectra extracted from the distribution of cooling data for both hadronic EoS models (left panel) and for hybrid stars with X-gap models I-IV (right panel). For comparison, the mass distribution of young, nearby NS from the population synthesis of Popov et al.⁸⁶ is shown at the bottom of the panels.

the critical density $n_c = 2.75 n_0 = 0.44 \text{ fm}^{-3}$.

In Fig. 7 we present temperature–age (TA) diagrams for two different hadronic models. Figure 9 shows the TA diagram for two hybrid star cooling models which are presented in Ref. 86. We note that the $T_m - T_s$ relationship between the temperatures of the inner crust and the stellar surface has been chosen according to a Tsuruta’s formula, for details see⁷⁵. The “TA test” is fulfilled when each data point ought to be explained with a cooling curve of an admissible configuration. The TA data points are taken from Ref. 64. The hatched trapeze-like region represents the brightness constraint (BC)⁶⁵. For each model nine cooling curves are shown for configurations with mass values corresponding to the binning of the population synthesis calculations explained in Ref. 86. A so called logN–LogS distribution constraint has been considered in Ref. 86 for the hybrid cooling scenario above, and it

has been suggested to use the marking of TA diagram with five grey values in order to encode the likelihood that stars in that mass interval can be found in the solar neighborhood, in accordance with the population synthesis scenario, see Fig. 9. The darkest grey value, for example, corresponds to the most populated mass interval 1.35 to 1.45 M_{\odot} predicted by the mass spectrum used in population synthesis. It has been suggested in Ref.66 that a mass spectrum can be derived from the sequences of TA curves of a given compact star cooling theory, see Fig. 10. This example demonstrates how in principle cooling simulations together with data from observation and population synthesis simulations could discriminate pairing patterns for quark matter phases. A recent review⁵² gives a flavor of the fascinating topics in the discussion of color superconducting phases in compact stars. Many new developments in the theory and observations of compact stars like, e.g., the discussion of single flavor⁸⁹ and strange quark matter⁹⁰ phases for providing possible deep crustal heating mechanisms to explain the puzzling phenomena of superbursts and cooling of X-ray transients^{91,92} will deepen our understanding of the high-density nuclear EoS.

Acknowledgments

We thank our collaborators, in particular H. Grigorian, G. Poghosyan, S. Popov, F. Sandin, and D. Voskresensky for their comments and for their contributions to the results reported here. D. Blaschke was supported in part by the Polish Ministry for Science and Higher Education under contract No. N N202 0953 33. T. Klähn is grateful for partial support from the Department of Energy, Office of Nuclear Physics, contract no. DE-AC02-06CH11357. The research of F. Weber is supported by the National Science Foundation under Grant PHY-0457329, and by the Research Corporation.

References

1. N. K. Glendenning, *Compact Stars, Nuclear Physics, Particle Physics, and General Relativity*, 2nd ed. (Springer-Verlag, New York, 2000).
2. F. Weber, *Pulsars as astrophysical laboratories for nuclear and particle physics*, Bristol, UK: IOP (1999).
3. *Physics of Neutron Star Interiors*, ed. by D. Blaschke, N. K. Glendenning, and A. Sedrakian, Lecture Notes in Physics **578** (Spring-Verlag, Berlin, 2001).
4. F. Weber, Prog. Nucl. Part. Phys. **54**, 193 (2005).
5. A. Sedrakian, Prog. Part. Nucl. Phys. **58**, 168 (2007).
6. D. Page and S. Reddy, Ann. Rev. Nucl. Part. Sci. **56**, 327 (2006).
7. F. Weber, R. Negreiros, P. Rosenfield, and M. Stejner, Prog. Nucl. Part. Phys. **59**, 94 (2007).
8. J. M. Lattimer and M. Prakash, Phys. Rept. **442**, 109 (2007).
9. J. Schaffner-Bielich, PoS (CPOD2007) 062 (2007), arXiv:0709.1043 [astro-ph].
10. D.J. Nice, E.M. Splaver, I.H. Stairs, O. Löhmer, A. Jessner, M. Kramer, and J.M. Cordes, Astrophys. J. **634**, 1242 (2005).
11. J. E. Trümper, V. Burwitz, F. Haberl and V. E. Zavlin, Nucl. Phys. Proc. Suppl. **132**, 560 (2004).

12. P. Kaaret *et al.*, *Astrophys. J.* **657**, L97 (2007).
13. T. Klähn *et al.*, *Phys. Rev. C* **74**, 035802 (2006).
14. T. Klähn *et al.*, *Phys. Lett. B* **654**, 170 (2007).
15. P. C. C. Freire, *AIP Conf. Proc.* **983**, 459 (2008).
16. S. E. Thorsett and D. Chakrabarty, *Astrophys. J.* **512**, 288 (1999).
17. G. Baym, C. Pethick, and P. Sutherland *Astrophys. J.* **170**, 299 (1971).
18. J. Walecka, *Ann. Phys. (N.Y.)* **83**, 491 (1974).
19. B. D. Serot and J. D. Walecka, *Adv. Nucl. Phys.* **16**, 1 (1986).
20. P.-G. Reinhard, *Rep. Prog. Phys.* **52**, 439 (1989).
21. P. Ring, *Prog. Part. Nucl. Phys.* **37**, 193 (1996).
22. T. Gaitanos, M. Di Toro, S. Typel, V. Baran, C. Fuchs, V. Greco, and H. H. Wolter, *Nucl. Phys. A* **732**, 24 (2004).
23. B. Liu, V. Greco, V. Baran, M. Colonna, and M. Di Toro, *Phys. Rev. C* **65**, 045201 (2002).
24. S. Typel, *Phys. Rev. C* **71**, 064301 (2005).
25. P. Danielewicz, R. Lacey, and W. G. Lynch, *Science* **298**, 1592 (2002).
26. G. E. Brown and M. Rho, *Phys. Rev. Lett.* **66**, 2720 (1991).
27. E. E. Kolomeitsev and D. N. Voskresensky, *Nucl. Phys. A* **759**, 373 (2005).
28. A. Akmal, V. R. Pandharipande, and D. G. Ravenhall, *Phys. Rev. C* **58**, 1804 (1998).
29. R. B. Wiringa, V. Fiks, and A. Fabrocini, *Phys. Rev. C* **38**, 1010 (1988).
30. B. Friedman and V. R. Pandharipande, *Nucl. Phys. A* **361**, 502 (1981).
31. E.N.E. van Dalen, C. Fuchs, and A. Faessler, *Nucl. Phys. A* **744**, 227 (2004); *Phys. Rev. C* **72**, 065803 (2005).
32. M. Baldo, G. F. Burgio and H. J. Schulze, *Phys. Rev. C* **61**, 055801 (2000).
33. P. Podsiadlowski, J. D. M. Dewi, P. Lesaffre, J. C. Miller, W. G. Newton, and J. R. Stone, *Mon. Not. Roy. Astron. Soc.* **361**, 1243 (2005).
34. M. Kramer *et al.*, *eConf C041213*, 0038 (2004).
35. A. J. Faulkner *et al.*, *Astrophys. J.* **618**, L119 (2005).
36. G. Bisnovatyi-Kogan, D. Blaschke, H. Grigorian, and S. Popov, *Mon. Not. Roy. Astron. Soc.* (2007) submitted.
37. F. S. Kitaura, H. T. Janka, and W. Hillebrandt, *Astron. Astrophys.* **450**, 345 (2006).
38. M. van der Klis, *ARA&A* **38**, 717 (2000).
39. M. C. Miller, *AIP Conf. Proc.* **714**, 365 (2004).
40. M. C. Miller, F. K. Lamb, and D. Psaltis, *Astrophys. J.* **508**, 791 (1998).
41. S. van Straaten, E. C. Ford, M. van der Klis, M. Méndez, and P. Kaaret, *Astrophys. J.* **540**, 1049 (2000).
42. W. Zhang, A. P. Smale, T. E. Strohmayer, and J. H. Swank, *Astrophys. J.* **503**, L147 (1998).
43. D. Barret, J. F. Olive, and M. C. Miller, *Mon. Not. Roy. Astron. Soc.* **361**, 855 (2005).
44. G. Lavagetto, I. Bombaci, A. D’Ai’, I. Vidana, and N. R. Robba, *arXiv:0612061 [astro-ph]*.
45. D. A. Leahy, S. M. Morsink, and C. Cadeau, *Astrophys. J.* **672**, 1119 (2008).
46. C. M. Miller, private communication (2007).
47. F. M. Walter and J. Lattimer, *Astrophys. J.* **576**, L145 (2002).
48. D. Kaplan, private communication (2006).
49. W. Ho, in *Proc. of the Int. Conf. on Isolated Neutron Stars: From the Interior to the Surface*, London, England, 24-28 Apr 2006; *Astrophys. Space Sci.* (2006) to be published.
50. J. Cottam, F. Paerels and M. Mendez, *Nature* **420**, 51 (2002).
51. F. Özel, *Nature* **441**, 1115 (2006).

16 *D. Blaschke, T. Klähn, and F. Weber*

52. M. Alford, et al., *Nature* **445**, E7 (2007).
53. M. Bejger, T. Bulik, and P. Haensel, *Mon. Not. Roy. Astron. Soc.* **364** (2005) 635.
54. J. M. Lattimer and B. F. Schutz, *Astrophys. J.* **629**, 979 (2005).
55. J. M. Lattimer and M. Prakash, *Science* **304**, 536 (2004).
56. M. Bejger, P. Haensel, and J. L. Zdunik, *Astron. Astrophys.* **464**, L49 (2007).
57. J. Madsen, *Phys. Rev. Lett.* **85**, 10 (2000).
58. A. Drago, G. Pagliara, and I. Parenti, *Astrophys. J.* **678**, L117 (2008).
59. G. S. Poghosyan, H. Grigorian, and D. Blaschke, *Astrophys. J.* **551**, L73 (2001).
60. N. Andersson and K. Kokkotas, *Int. J. Mod. Phys. D* **10**, 381 (2001).
61. N. K. Glendenning and F. Weber, *Astrophys. J.* **559**, L119 (2001).
62. D. Blaschke, I. Bombaci, H. Grigorian, and G. S. Poghosyan, *New Astron.* **7**, 107 (2002).
63. H. Grigorian, D. Blaschke, and G. S. Poghosyan, *Nucl. Phys. A* **715**, 831 (2003).
64. D. Page, J. M. Lattimer, M. Prakash, and A. W. Steiner, *Astrophys. J. Suppl.* **155**, 623 (2004).
65. H. Grigorian, *Phys. Rev. C* **74**, 025801 (2006).
66. D. Blaschke and H. Grigorian, *Prog. Part. Nucl. Phys.* **59**, 139 (2007).
67. E. P. J. Heuvel, AIP Conf. Proc., eds. L. Burderi et al., arXiv:0704.1215 [astro-ph].
68. C. D. Roberts and S. M. Schmidt, *Prog. Part. Nucl. Phys.* **45**, S1 (2000).
69. D. Nickel, J. Wambach and R. Alkofer, *Phys. Rev. D* **73**, 114028 (2006).
70. H. Chen, W. Yuan, L. Chang, Y. X. Liu, T. Klähn, and C. D. Roberts, arXiv:0807.2755 [nucl-th].
71. D. Blaschke, S. Fredriksson, H. Grigorian, A. M. Öztas and F. Sandin, *Phys. Rev. D* **72**, 065020 (2005).
72. S. B. Rüster, V. Werth, M. Buballa, I. A. Shovkovy and D. H. Rischke, *Phys. Rev. D* **72**, 034004 (2005).
73. H. Abuki and T. Kunihiro, *Nucl. Phys. A* **768**, 118 (2006).
74. H. J. Warringa, D. Boer and J. O. Andersen, *Phys. Rev. D* **72**, 014015 (2005).
75. D. Blaschke, H. Grigorian, and D. N. Voskresensky, *Astron. Astrophys.* **424**, 979 (2004).
76. D. Blaschke, H. Grigorian, and D. N. Voskresensky, *Astron. Astrophys.* **368**, 561 (2001).
77. D. N. Voskresensky, *Lect. Notes Phys.* **578**, 467 (2001).
78. A. Sedrakian, arXiv:0701017 [astro-ph].
79. E. E. Kolomeitsev and D. N. Voskresensky, *Phys. Rev. C* **77**, 065808 (2008).
80. P. Jaikumar and M. Prakash, *Phys. Lett. B* **516**, 345 (2001).
81. D. Blaschke, T. Klähn, and D. N. Voskresensky, *Astrophys. J.* **533**, 406 (2000).
82. T. Takatsuka and R. Tamagaki, *Prog. Theor. Phys.* **112**, 37 (2004).
83. A. Schwenk and B. Friman, *Phys. Rev. Lett.* **92**, 082501 (2004).
84. H. Grigorian and D. N. Voskresensky, *Astron. Astrophys.* **444**, 913 (2005).
85. H. Grigorian, D. Blaschke, and D. Voskresensky, *Phys. Rev. C* **71**, 045801 (2005).
86. S. Popov, H. Grigorian and D. Blaschke, *Phys. Rev. C* **74**, 025803 (2006).
87. D. Blaschke, D. N. Voskresensky, and H. Grigorian, *Compact Stars. The Quest for New States of Dense Matter*, World Scientific, Singapore (2004), p. 409.
88. S. Popov, H. Grigorian, R. Turolla, and D. Blaschke, *A&A* **448**, 327 (2006).
89. D. Blaschke, F. Sandin, T. Klähn and J. Berdermann, arXiv:0807.0414 [nucl-th].
90. D. Page and A. Cumming, *Astrophys. J.* **635**, L157 (2005).
91. M. Stejner and J. Madsen, *Astron. Astrophys.* **458**, 523 (2006).
92. P. S. Shternin, D. G. Yakovlev, P. Haensel and A. Y. Potekhin, *Mon. Not. R. Astron. Soc.* **382**, L43 (2007).